



# Classification and variation of fracture modes in laser shock hole-clinching

Chao Zheng<sup>1</sup> · Shushuai Liu<sup>1</sup> · Yunhu Zhu<sup>2</sup> · Yiliang Zhang<sup>1</sup> · Guoqun Zhao<sup>1</sup> · Zhong Ji<sup>1</sup>

Received: 22 May 2020 / Accepted: 13 April 2021 / Published online: 19 April 2021  
© The Author(s), under exclusive licence to Springer-Verlag London Ltd., part of Springer Nature 2021

## Abstract

Laser shock hole-clinching is a high-strain rate mechanical joining process in which the metal foils are joined together based on plastic deformation generated by a laser-induced shock wave. In the process, fracture is a typical defect and seriously influences the clinching quality and production efficiency of joints. However, the classification and variation of fracture modes in laser shock hole-clinching are of less concern. In this study, the fracture mode of Cu-Fe joints in laser shock hole-clinching was experimentally investigated. Both optical microscopy and scanning electron microscopy were adopted to analyze the fracture surface morphology of clinched joints. The influence of laser power density, laser spot diameter, the initial grain size and thickness of metal foil, and spacer height on the fracture mode of joints was evaluated. It is revealed that the temperature increase caused by high-strain rate plastic deformation has no impact on the fracture behavior of the joining partners. Fracture always occurs on joining partner I, and it can be divided into four modes, including bottom surface fracture, bottom corner fracture, neck fracture, and mixed fracture. It is found that fracture on the bottom surface is seldom seen but mixed fracture accounts for most of the cracked specimens. Neck tensile fracture rarely appears alone, and it usually exists accompanied by fracture on the bottom corner. The fracture mode varies from a tensile fracture mode on the bottom corner to a mixed fracture mode and then to a shear fracture mode on the neck with the enhancement of laser power density. In addition, the initial grain size of joining partner I has a significant impact on the fracture mode of clinched joints. The fracture mode varies from bottom corner fracture to mixed fracture in relation to the change of mechanical properties of metal foil with an enlarged grain size. However, the mixed fracture mode always appears with the enlargement of both laser spot diameter and spacer height.

**Keywords** Laser shock forming · Laser shock clinching · Fracture mode · Fracture surface morphology

## 1 Introduction

Laser shock hole-clinching is one of mechanical joining processes in which at least one metal foil is plastically deformed to form an interlock structure. The process originates from laser shock forming of metal foils and holds the technological

advantages of laser shock forming and clinching. Since the joint is obtained based on plastic deformation, laser shock hole-clinching is especially suitable for the joining of dissimilar materials with significant differences in physical properties, such as melting point, thermal conductivity, plasticity, and yield strength.

The mechanism of laser shock hole-clinching is illustrated in Fig. 1a. A laser beam with a nanosecond pulse duration and a laser power density of up to  $10^{12}$  W/m<sup>2</sup> level is employed as a punch. While the laser beam arrives on the top surface of the absorbent coating, the coating material absorbs the incident laser energy and then immediately forms a plasma with high pressure and temperature [1]. Due to the confinement of the confining layer, the generated plasma cannot escape freely and will rapidly expand towards the joining partners, leading to the formation of a shock wave. The shock wave subsequently propagates into joining partner I and further causes plastic deformation when the amplitude of the shock wave

✉ Chao Zheng  
zhengchao@sdu.edu.cn

<sup>1</sup> Key Laboratory for Liquid-Solid Structural Evolution and Processing of Materials (Ministry of Education), School of Materials Science and Engineering, Shandong University, Jinan 250061, People's Republic of China

<sup>2</sup> Key Laboratory of Extraordinary Bond Engineering and Advanced Materials Technology, School of Materials Sciences and Engineering, Yangtze Normal University, Chongqing 408100, People's Republic of China

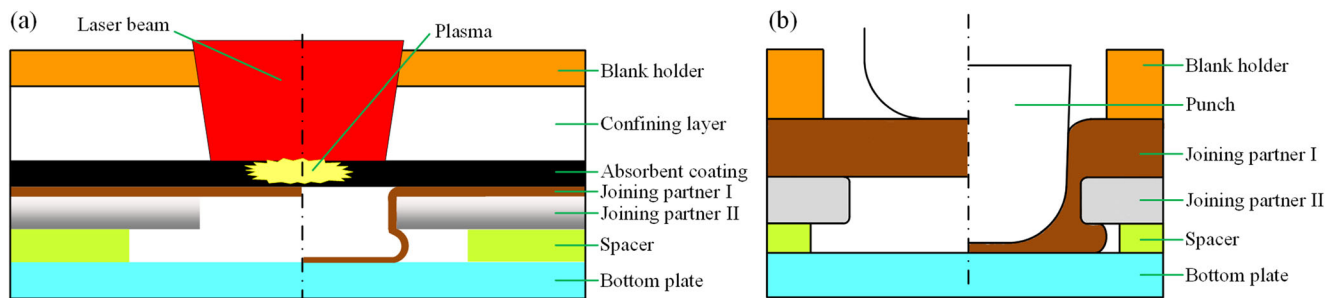


**Fig. 1** Schematic diagram of laser shock hole-clinching process (a) and conventional hole-clinching process (b)

pressure is beyond the yield strength of the material [2]. Because of the effect of the shock wave, joining partner I flows into the pre-pierced hole on joining partner II, and finally, the partners are joined together at high strain rates. Usually tens to hundreds of pulses are needed to accomplish the process depending on the material properties and pulsed laser parameters. It is noted that the laser-induced shock wave is responsible for the joining of metal foils in the laser shock hole-clinching process, which exhibits significant differences in the fundamental mechanism in comparison to the laser welding process. The other compositions of the experimental apparatus and their roles in the laser shock hole-clinching process are similar to those in laser shock forming [3]. Unlike a rigid punch used in the conventional hole-clinching, the laser-induced shock wave is adopted to act as a flexible punch, as illustrated in Fig. 1. In this case, the spot diameter can be easily adjusted according to the different dimensions of the pre-pierced hole on joining partner II. The energy level of the laser beam is able to be precisely controlled by using a laser system based on the joining requirement of partners with various mechanical properties. Therefore, the process possesses the technological superiority of non-contact, flexibility, controllability, and high precision.

The clinching feasibility of metal foils by a laser-induced shock wave and the influence of process parameters on interlock formation have attracted much more attention. The combinations of aluminum/stainless steel [4, 5], aluminum/copper [5, 6], and copper/stainless steel [7] are successfully joined together under a shock wave. It is found that the application of a pulsed laser beam is appropriate for the joining requirements of metallic materials with a thickness in the micron range [8]. Moreover, the effects of the number of pulses [4, 7, 8], laser energy [5–7], thickness of the absorbent coating [6], spacer height [7], and shock wave pressure [9] on the mechanical joining behavior of metal foils have been explored through experimental and numerical approaches. The investigations show that the evolution of the interlock structure and the strength of the clinched joint are sensitive to process parameters, indicating that the reasonable choice of parameters is important to

obtain a joint with high quality during laser shock hole-clinching. The recent advance in laser shock hole-clinching includes the realization of three joining partners [10], the achievement of a line interlock structure [11], and the development of the micro-shear clinching process [12].

Fracture is one of main defects in laser shock forming due to the low stiffness and small thickness of metal foils, the complex stress state during deformation, and the ultrahigh shock wave pressure, especially because of the unreasonable arrangement of process parameters. Thus, the fracture behavior and modes are necessary to identify firstly to further eliminate this defect. Li et al. [13] employed the Johnson-Cook failure model to numerically simulate the fracture behavior of materials in laser shock forming. It is found that the thickness reduction of the foil near the fracture region can be up to 80% owing to the effect of tensile stress. Wielage and Vollertsen [14] analyzed the fracture behavior of metal foils during drawing by multiple laser pulses. It is concluded that fracture may occur on the bottom surface, the bottom corner, or the entrance corner depending on the number of laser pulses. Liu et al. [15] carried out morphological analysis of a fracture surface in a multiple-pulse laser shock bulging process. The examinations show that there are four fracture modes based on the various fracture mechanisms, that is, tensile fracture, shear fracture, mixed fracture, and spallation. Wang et al. [16] observed that fracture is inclined to appear on the bottom surface caused by serious local thinning in the laser shock hydraulic bulging process, especially at a very high laser power density. Both the large tensile stress and relatively free flowing of bottom material lead to the fracture on the bottom. Zhang et al. [17] presented a comparative study on the fracture behavior of AZ31 magnesium alloy and molybdenum in multiple-pulse laser shock forming. Based upon examinations, it is noted that both AZ31 and molybdenum exhibit significant thickness thinning on fracture sites, whereas spallation is also observed for molybdenum. Jiang et al. [18] revealed that there are three fracture mechanisms for aluminum alloy in laser shock forming, including spallation, excessive thinning, and mixed mechanism. The abovementioned researches give a constructive understanding of fracture defect in the laser shock

forming process, which is beneficial for further controlling and improving the forming quality of parts.

Furthermore, the change of fracture modes in relation to deformation conditions has been investigated to make a deep exploration of the fracture behavior in laser shock forming. Zheng et al. [19] evaluated the response of metal foils under different ratios of the laser beam diameter to die hole diameter in the laser shock punching process. It is certain that the fracture mode varies from shear to mixed mode and then to tensile as the ratio decreases. Shen et al. [20] established a finite element model to simulate the fracture behavior of metal foils in laser shock forming with the aid of a rubber sheet. The numerical results show that while the laser energy is enhanced from 1380 to 1690 mJ, the fracture mode is changed from tensile tearing to shear rupture. In their further work, morphological analysis of the fracture surface by scanning electron microscopy under different laser energies was conducted [21]. It is found that while the laser energy is increased to 1900 mJ, the filament fracture mode appears, indicating that the superplastic flowing of metal foil occurs prior to fracture. Li et al. [22] discussed the effect of shock wave pressure on fracture behavior in the laser shock punching process. It is observed that although the metal foil is always separated by shear mode, the edge of the punched hole is smoother and the plug height is lower with the enhancement of the induced shock wave pressure.

However, fewer attempts are made towards the classification of fracture modes in laser shock hole-clinching and the examination of fracture surface morphology to deeply explore the fracture mechanism on the micron scale. It is obvious that both the material plastic flowing and stress state are more complex in clinching due to the specific geometry of joints, implying that the fracture behavior may exhibit different characteristics in comparison to laser shock forming. Moreover, the influence of critical process parameters, such as laser power density, laser spot diameter, initial grain size and thickness of metal foil, and spacer height, on the fracture mode of joints in laser shock hole-clinching is also of less concern. In this

sense, it is full of the importance to reveal the classification and variation of fracture modes in laser shock hole-clinching through a detailed investigation.

In this study, the fracture mode of dissimilar material joints by laser shock hole-clinching was investigated. T2 pure copper and 304 stainless steel foils were joined together under a laser-induced shock wave. Both optical microscopy (OM) and scanning electron microscopy (SEM) were adopted to analyze the fracture surface morphology of joints. The temperature increase during clinching was assessed considering the plastic deformation at high strain rates. The influence of critical process parameters on the fracture mode of joints was evaluated in detail.

## 2 Experiments

### 2.1 Experimental setup

A Nd:YAG laser system (Nimma-900, Beamtech Optronics Co., Ltd.) was employed to conduct the laser shock hole-clinching experiments. The diameter of the laser beam converging on the metal surface can be changed by adjusting the distance between the lens and the metal foil. The output laser energy was measured using a digital energy meter (FieldMaxII-TOP, Coherent). The pulse frequency was set to 1 Hz. Optical quartz glass with a thickness of 3 mm was chosen to serve as the confining layer, and ink was used as the absorbent coating, which contains carbon powders, organic promoters, and solvent. The ink was carefully pre-coated on the glass surface facing the metal foil, and the average thickness was 80 μm. While every five laser pulses were applied, the position of the quartz glass was adjusted by a small displacement to ensure the protection of the ink. The location of every component refers to Fig. 1. Table 1 summarizes the detailed process parameters in experiments. The laser power density  $I$  depends on the pulsed laser energy  $E$ , the laser spot diameter  $d_s$ , and the pulse duration  $\tau$ , expressed as  $I = 4E/\pi d_s^2 \tau$ .

**Table 1** Detailed process parameters in experiments

Parameter	Unit	Value
Laser wavelength ( $f$ )	nm	1064
Pulse duration ( $\tau$ )	ns	7.5
Laser energy per pulse ( $E$ )	mJ	100, 110, 120, 130, 150
Laser power density ( $I$ )	$\times 10^{12}$ W/m <sup>2</sup>	4.25, 4.67, 5.10, 5.52, 6.37 (at $d_s = 2.0$ mm)
Laser spot diameter ( $d_s$ )	mm	1.8, 2.0, 2.2
Pre-pierced hole diameter ( $d_p$ )	mm	2.0
Ratio of $d_s$ to $d_p$ ( $M$ )	/	0.9, 1.0, 1.1
Thickness of T2 pure copper foil ( $t_U$ )	μm	30, 50
Thickness of 304 stainless steel foil ( $t_L$ )	μm	100
Spacer height ( $H$ )	μm	100, 150, 200
Initial grain size of pure copper ( $d_G$ )	μm	13, 17, 27 (at $t_U = 30$ μm)

## 2.2 Specimen preparation

T2 pure copper foil with a thickness of 30 and 50 μm was chosen as joining partner I, while 304 stainless steel with a thickness of 100 μm was used to act as joining partner II. Before the laser shock hole-clinching process, laser drilling with a fiber laser cutting machine (SF3015, Senfeng Laser Technology Co., Ltd.) was adopted to fabricate a round hole 2.0 mm in diameter on 304 steel foil. In the previous experiments, it is concluded that there was no obvious evidence of plastic deformation for joining partner II during the process [7]. Therefore, only joining partner I needs a series of heat treatments in order to obtain various initial grain sizes to verify their effect on fracture modes. The as-received pure copper foil of 30 μm in thickness was annealed in a vacuum furnace at temperatures of 450, 600, and 750 °C for 1 h, and then the average grain sizes in the thickness direction were measured using an optical microscope (GX51, Olympus) by the mean linear intercept method according to the ASTM E112 standard. Figure 2 presents microstructures of pure copper foil after different heat treatments. The initial grain size was 13, 17, and 27 μm on average.

After the laser shock hole-clinching process, the macro-morphology of the fracture surface was observed using an ultra-depth digital microscope with data processing software (DX-200, Shanghai Yongao Precision Instrument Co., Ltd.). A scanning electron microscope (JSM-7800F, JEOL) with an energy-dispersive spectrometer system (X-Max 80, Oxford) was adopted to characterize the micro-morphology of the fracture surface.

## 3 Methodology

### 3.1 Evaluation of temperature increase during laser shock

While the materials are impacted by shock loading, the distance of heat transfer originating from plastic deformation is generally limited, and then the adiabatic shear phenomenon may occur, which plays an important role in the fracture behavior of materials [23, 24]. Therefore, it is necessary to evaluate the temperature increase during the laser shock hole-clinching process and discuss its effect on the fracture mode of metal foils.

The temperature increase Δ*T* induced by plastic deformation under laser-induced shock wave loading can be expressed as [25]

$$\Delta T = \frac{\beta}{\rho C_p} \int_0^\epsilon \sigma d\epsilon \tag{1}$$

where β is the coefficient of plastic work converting into heat, ρ is the material density, and *C<sub>p</sub>* is the isobaric specific heat. In

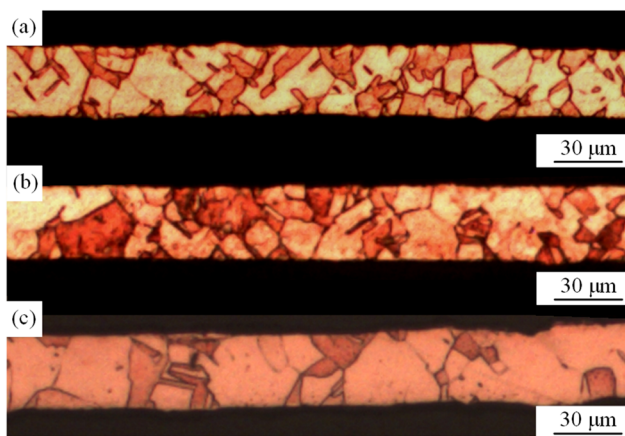


**Fig. 2** Microstructures of pure copper foil with a thickness of 30 μm after various heat treatments. **a** 450 °C, 1 h. **b** 600 °C, 1 h. **c** 750 °C, 1 h

laser shock processes, the Johnson-Cook constitutive model is generally used to describe the relationship of stress σ and plastic strain ε [26]:

$$\sigma = (A + B\epsilon^n) \left( 1 + C \ln \frac{\dot{\epsilon}}{\dot{\epsilon}_0} \right) \left[ 1 - \left( \frac{T - T_r}{T_m - T_r} \right)^m \right] \tag{2}$$

where *A*, *B*, and *C* are material constants; *n* is the strain hardening index; ε̇ is the strain rate; ε̇<sub>0</sub> is the reference strain rate; *T<sub>r</sub>* is the room temperature; *T<sub>m</sub>* is the melting point of the material; and *m* is the thermal softening index. Thus, Δ*T* can be calculated by

$$\Delta T = \left\{ 1 - \exp \left[ - \frac{\beta \left( 1 + C \ln \frac{\dot{\epsilon}}{\dot{\epsilon}_0} \right)}{\rho C_p (T_m - T_r)} \times \left( A\epsilon + \frac{B\epsilon^{n+1}}{n+1} \right) \right] \right\} \times (T_m - T_r) \tag{3}$$

### 3.2 Estimation of laser-induced shock wave pressure

In the confining condition, the laser-induced shock wave pressure can be estimated by [27]

$$P_{\max} = 10^{-9} \sqrt{\left( \frac{a}{2a+3} \right) \cdot Z \cdot I} \tag{4}$$

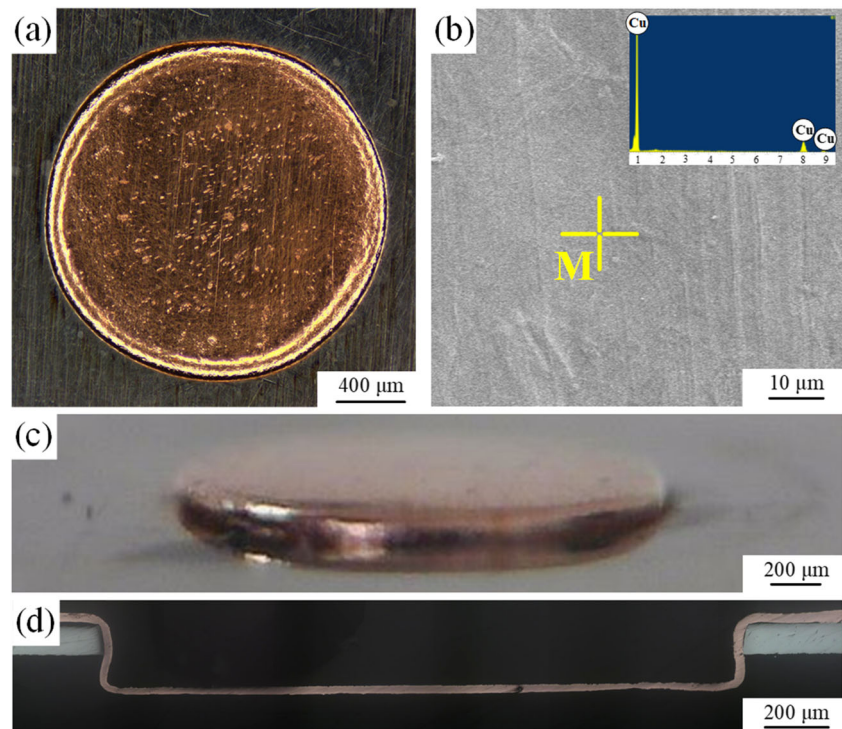
where *P<sub>max</sub>* is the peak value of the shock wave pressure; *a* is the energy conversion coefficient, generally regarded as 0.1; *I* is the laser power density; and *Z* is the shock impedance related to the interaction between the metal foil *Z*<sub>1</sub> and the confining overlay *Z*<sub>2</sub>, expressed as 2/*Z* = 1/*Z*<sub>1</sub> + 1/*Z*<sub>2</sub>.

## 4 Results and discussion

### 4.1 Morphology of clinched joint

After all of arranged laser pulses have been exerted, the residual ink splashed on the joint surface during material-laser interaction was removed by a heated ultrasonic cleaner, and then anhydrous alcohol was used to clean the joint surface. The typical morphology of the qualified clinched joint is shown in Fig. 3. The corresponding clinching conditions are as follows:  $I = 5.52 \times 10^{12} \text{ W/m}^2$ ,  $d_G = 17 \text{ }\mu\text{m}$ ,  $t_U = 30 \text{ }\mu\text{m}$ ,  $d_S = 2.0 \text{ mm}$ , and  $H = 100 \text{ }\mu\text{m}$ . A total of 30 pulses were applied during clinching. It is clearly seen that a round joint with good geometry has been achieved, as shown in Fig. 3 a and c. For the sake of careful examination of the surface morphology, an amplified observation of the joint surface facing laser beam was implemented by SEM, and a further element analysis of point M near the center of the joint was conducted using an energy-dispersive spectrometer (EDS). According to Fig. 3b, obviously there is no evidence of laser ablation on the joint surface, such as voids, cracks, or melted droplets. Moreover, the EDS result shows that the surface is composed of Cu, suggesting that the laser shock hole-clinching process is a mechanical joining technology and the formation of dissimilar material joints is accomplished with the action of a laser-induced shock wave. The transverse morphology of the joint is shown in Fig. 3d. It can be seen that an interlock structure is obtained through the plastic deformation of joining partner I.

**Fig. 3** Morphology of the qualified joint. **a** Top view of the joint. **b** Amplification of the center of joining partner I (the inset is EDS result of point M). **c** Side view of the joint. **d** Transverse morphology of the joint



### 4.2 Evaluation of temperature increase in laser shock hole-clinching

The temperature change of metal foil during plastic deformation in laser shock hole-clinching can be assessed through Eq. (2). For pure copper,  $\beta = 0.9$ ,  $\rho = 8.9 \times 10^3 \text{ kg/m}^3$ ,  $C_p = 383 \text{ J/(kg K)}$ ,  $A = 90 \text{ MPa}$ ,  $B = 292 \text{ MPa}$ ,  $n = 0.31$ ,  $C = 0.025$ ,  $\dot{\varepsilon}_0 = 1.0/\text{s}$ ,  $m = 1.09$ ,  $T_m = 1356 \text{ K}$ , and  $T_r = 298 \text{ K}$  [28]. The strain rate of metal foil in pulsed laser shock loading can be regarded as  $10^3/\text{s}$  based on an experimental detection [29]. According to the calculation conducted by Veenas and Vollertsen, the first laser pulse can lead to an average strain of 0.03, which is the largest strain per pulse among the applied laser pulses [4]. Thus, the temperature increase arising from plastic deformation is about 2.1 K. This result is close to the value of the temperature increase due to plastic deformation in the laser shock process evaluated by Ye et al. [30], indicating that there is no obvious influence of temperature increase on the fracture behavior of the joining partners.

### 4.3 Classification of fracture modes

Based upon the careful examination of defective clinched joints, it is found that fracture always occurs on joining partner I and may appear on the bottom surface, bottom corner, and neck of the joint. Moreover, in some cases mixed fracture may appear combining bottom corner fracture and neck fracture.

The surface morphology of each fracture mode was observed, and the corresponding fracture mechanism was analyzed.

#### 4.3.1 Fracture on bottom surface

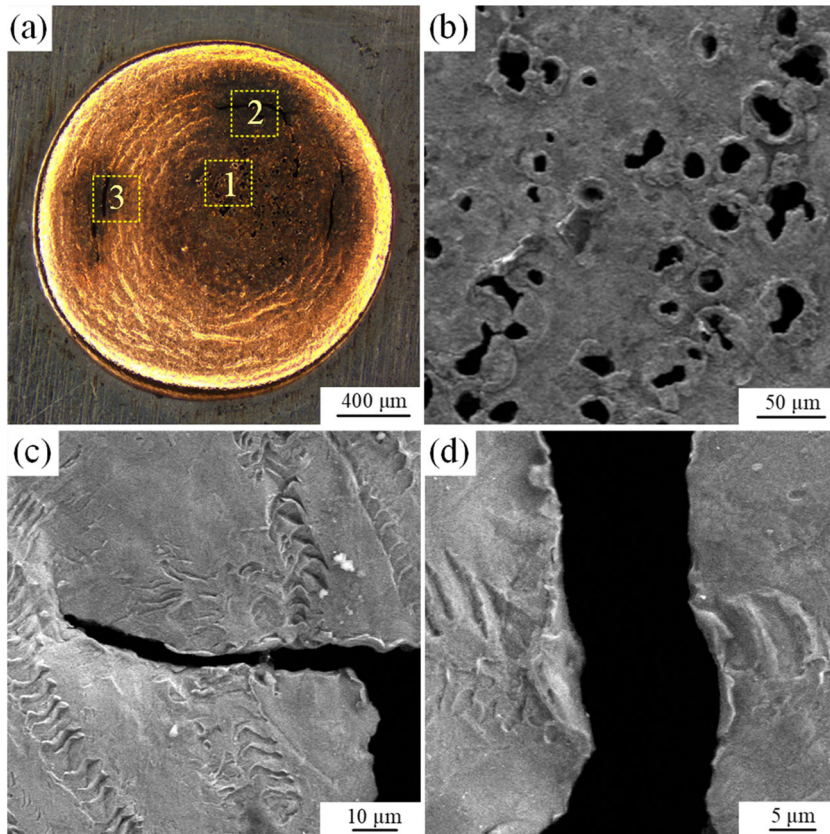
Figure 4 presents the fracture morphology on bottom surface of the joint. The corresponding clinching conditions are as follows:  $I = 4.25 \times 10^{12} \text{ W/m}^2$ ,  $d_G = 13 \text{ }\mu\text{m}$ ,  $t_U = 30 \text{ }\mu\text{m}$ ,  $d_S = 2.0 \text{ mm}$ , and  $H = 100 \text{ }\mu\text{m}$ . The total number of laser pulses was 80. It can be apparently seen that there are lots of voids scattered on the bottom surface as well as cracks, seen in Fig. 4a. This phenomenon is different from the typical fracture morphology in the laser shock forming process in which only cracks appear [14, 16, 18]. Figure 4b presents the amplification of region 1 in Fig. 4a. It can be seen that the dimension of voids is in the range of 10–40  $\mu\text{m}$  with irregular geometry. Figure 4c and d further examine the morphology of regions 2 and 3 in Fig. 4a, respectively. Note that the neighboring region of cracks is quite rough, implying that the material undergoes large plastic deformation during the process. In addition, it is found that fracture on the bottom surface is seldom seen among the fractured joints, since in this case a relatively low laser power density and quite a lot of pulses are usually needed.

In order to understand the reason for the formation of voids on the bottom surface, the morphology of the joint

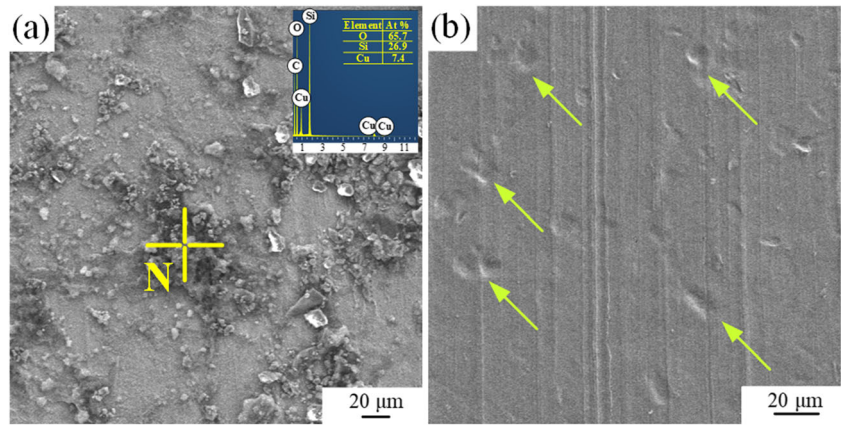
before and after removal of residual absorbent coating on the bottom surface is observed, as shown in Fig. 5. The applied laser power density was  $4.25 \times 10^{12} \text{ W/m}^2$  with a total of 40 pulses. It can be seen that after the interaction between the pulsed laser beam and coating material, there are plenty of granular residual substances on the bottom surface facing laser irradiation; refer to Fig. 5a. The EDS result of point N shows that these substances are composed of Si, C, and O elements besides Cu. While the residual substances were removed, many dents have been left with a size in the micron range, as seen in Fig. 5b. This phenomenon suggests that the granular substances are related to the emergence of dents and subsequent formation of voids while more laser pulses are applied.

Figure 6 illustrates the formation process of voids on the bottom surface of the joint in laser shock hole-clinching. Before laser irradiation, ink was pre-coated on the glass surface facing the metal foil, which contains carbon powders, organic promoters, and solvent. While a laser beam irradiates the ink, part of the ink immediately absorbs the laser energy and forms a plasma, as seen in Fig. 6(a). This interaction mainly relies on the applied laser power density and the absorbing capacity of the coating material. Obviously, less ink will be consumed with a relatively low laser power density. The rapid expansion of the plasma

**Fig. 4** Morphology of fracture on bottom surface. **a** General view of the bottom. **b** Amplification of region 1 in **a**. **c** Amplification of region 2 in **a**. **d** Amplification of region 3 in **a**



**Fig. 5** Morphology of the joint before (a) and after (b) removal of residual absorbent coating material on the bottom surface. The inset in a is the EDS result of point N



generates a shock wave and then leads to metal foil deformation. Meanwhile, some particles consisting of carbide and silicide which do not react with the incident laser will fly along the propagation direction of the shock wave and then impact the bottom surface at a high velocity; refer to Fig. 6(b). Some positions on the bottom surface will become thinner through the continuous collision of particles, as shown in Fig. 6(c). Finally, voids appear in excessive thinning positions under the effect of further impact, as seen in Fig. 6(d).

### 4.3.2 Fracture on bottom corner

Figure 7 presents the fracture morphology on the bottom corner of the joint. The corresponding clinching conditions are as follows:  $I = 4.67 \times 10^{12} \text{ W/m}^2$ ,  $d_G = 17 \text{ μm}$ ,  $t_U = 30 \text{ μm}$ ,  $d_S = 2.0 \text{ mm}$ , and  $H = 100 \text{ μm}$ . The total number of laser pulses was 60. Figure 7 b–d give an amplifying examination of region 1 in Fig. 7 a and show different characteristics on the fracture surface. As shown in Fig. 7b and c, two interesting phenomena can be seen on fracture surface, that is, slip traces and serrated fracture boundaries, which are also noted in laser

shock forming of metal foil [21]. In the experiment, it is found that after 35 pulses have been applied with a laser power density of  $4.67 \times 10^{12} \text{ W/m}^2$ , an interlock structure starts forming and its value becomes larger with the increase of laser pulses. In this case, a considerable plastic deformation takes place prior to fracture, leading to the occurrence of slip traces on the fracture surface. In addition, the fracture surface in Fig. 7d exhibits significant thinning, indicating that tensile stress plays an important role in this fracture mode [18]. Figure 8 illustrates the force acting on the bottom corner in laser shock hole-clinching. It can be seen that in the interlock formation stage, joining partner I expands along the  $r$  direction due to the confinement of the bottom plate along the  $z$  direction. In such a condition, the material in the bottom corner suffers from bilateral tensile stresses and its plastic deformation continues through the reduction in thickness, which is similar to those in the conventional mechanical clinching process [31]. As the laser pulses increase, the contact area of joining partner I and the bottom plate becomes larger, resulting in the difficulty of material flow. Therefore, the further radial expansion leads to fracture in this location because of excessive thinning at the corner.

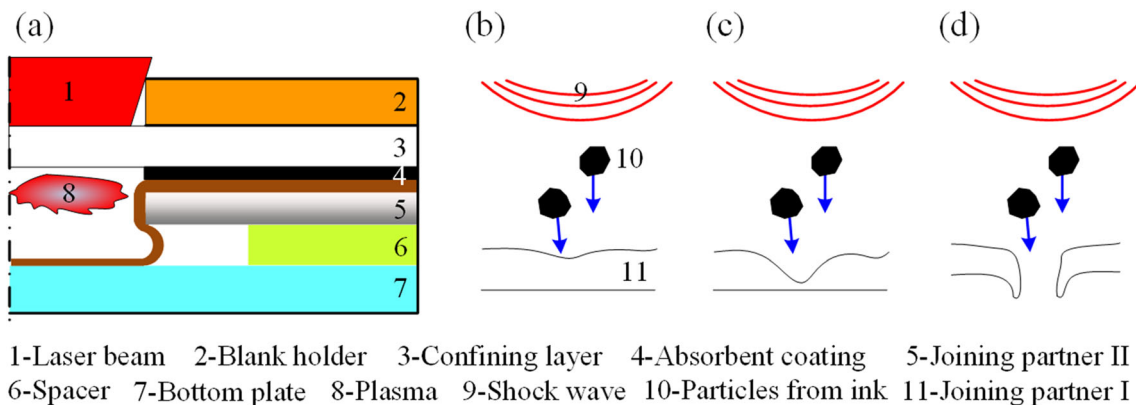
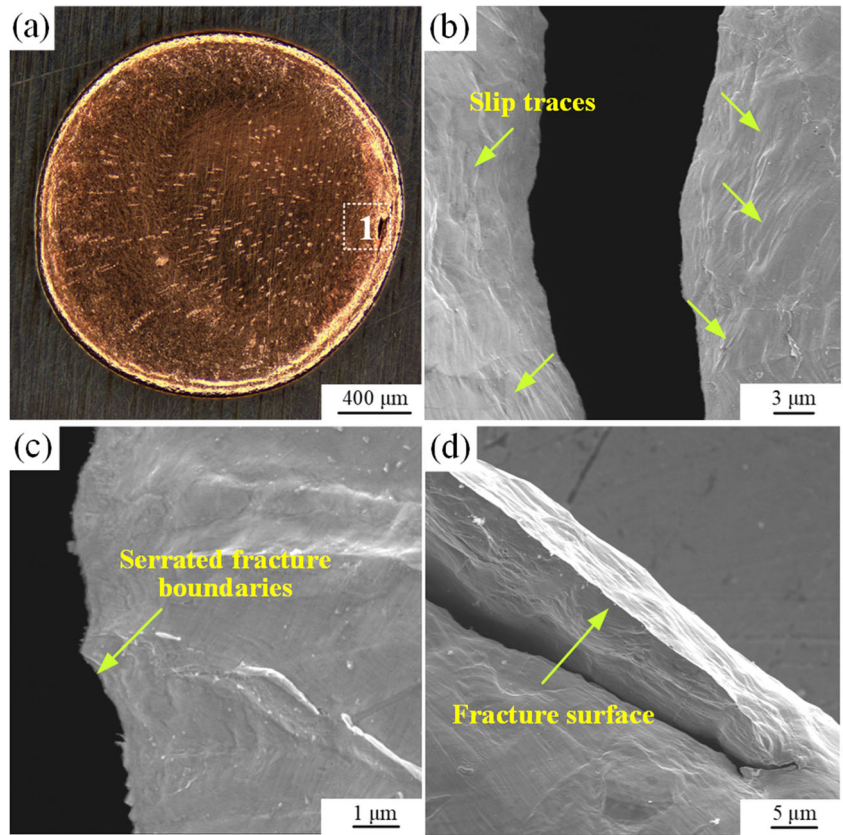


**Fig. 6** Formation illustration of voids on the bottom surface of joint: (a) generation of plasma; (b) impact between particles from ink and bottom surface; (c) local thinning on the bottom surface; (d) final formation of voids

**Fig. 7** Morphology of fracture on bottom corner. **a** General view of the joint bottom. **b** Slip traces on fracture surface. **c** Serrated fracture boundaries. **d** The end of a crack

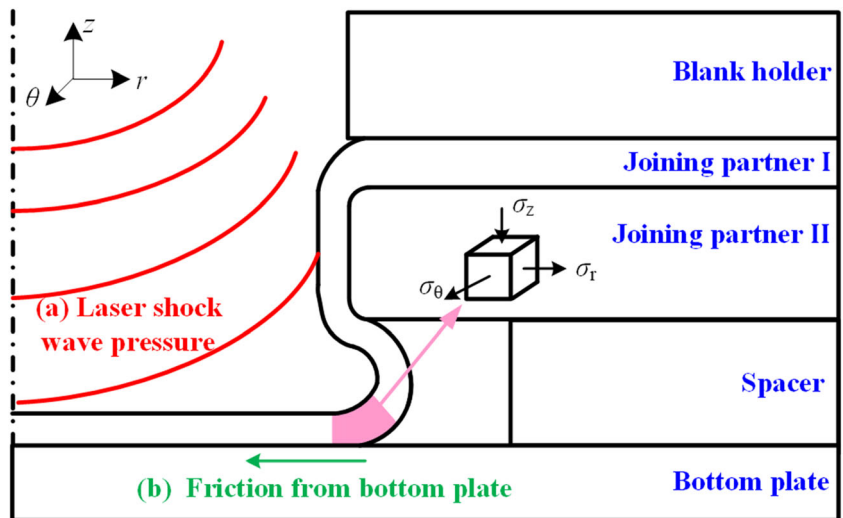


**4.3.3 Fracture on neck**

Figure 9 presents the fracture morphology on the neck of the joint. The corresponding clinching conditions are as follows:  $I = 5.10 \times 10^{12} \text{ W/m}^2$ ;  $d_G = 17 \text{ μm}$ ;  $t_U = 30 \text{ μm}$ ;  $d_S = 2.0 \text{ mm}$ ;  $H = 100 \text{ μm}$ ; and number of laser pulses, 50. Note that joining partner II has been carefully removed to better observe the fracture surface on joining partner I.

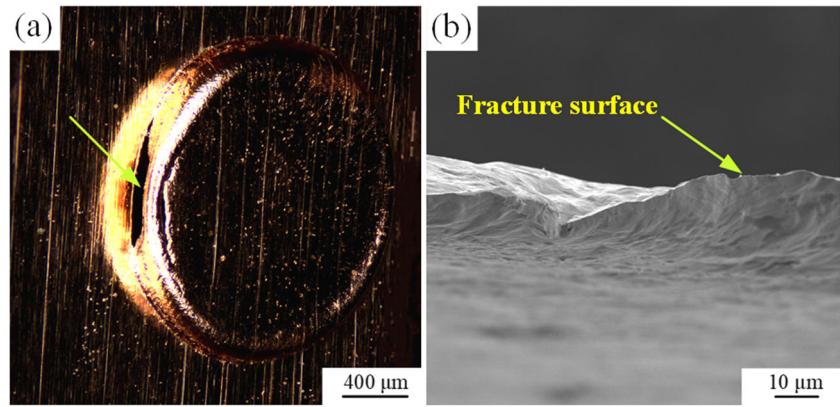
From Fig. 9a, it can be seen that the crack occurs near the upper corner of joining partner II. As seen in Fig. 9b, it is manifest that there is serious thinning within the fracture region, indicating that a considerable amount of plastic deformation takes place before fracture and the deformed metal foil is too thin to sustain the effect of tensile stress. This fracture mode is also observed in the conventional mechanical clinching process of metallic plates based on

**Fig. 8** Force acting on bottom corner in laser shock hole-clinching





**Fig. 9** Morphology of fracture on neck. **a** General view of the fracture region. **b** Amplification of fracture surface



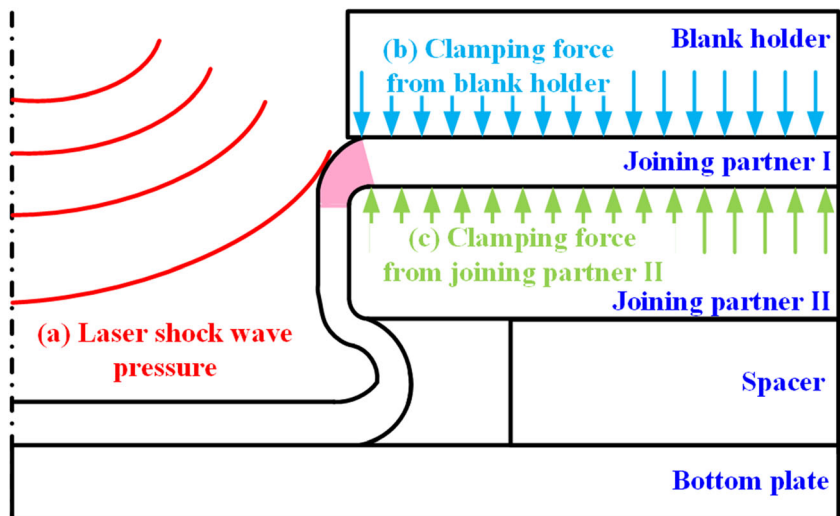
the same micro-fracture mechanism [32]. However, in the experiments, it is found that the neck fracture rarely appears alone. In fact, it usually exists accompanied by fracture on the bottom corner.

Figure 10 illustrates the force acting on the region in contact with the upper corner of joining partner II. Before the laser shock hole-clinching process, both joining partners I and II are compressed tightly by the blank holder, and thus, the material of partner I outside the pre-pierced hole will keep its position during laser shock. In this case, there is no material flowing into the pre-pierced hole and plastic deformation of joining partner I develops, resulting from the thickness reduction of the material within the pre-pierced hole. It is noted that the material near the upper corner of joining partner II undergoes complex deformation, that is, bending followed by stretching forming. Thus, local thinning is inclined to appear in this region. In addition, the pre-pierced hole on joining partner II is manufactured by the laser drilling process, and the small radius of the upper corner of joining partner II may also cause an adverse impact on the local load-bearing capacity.

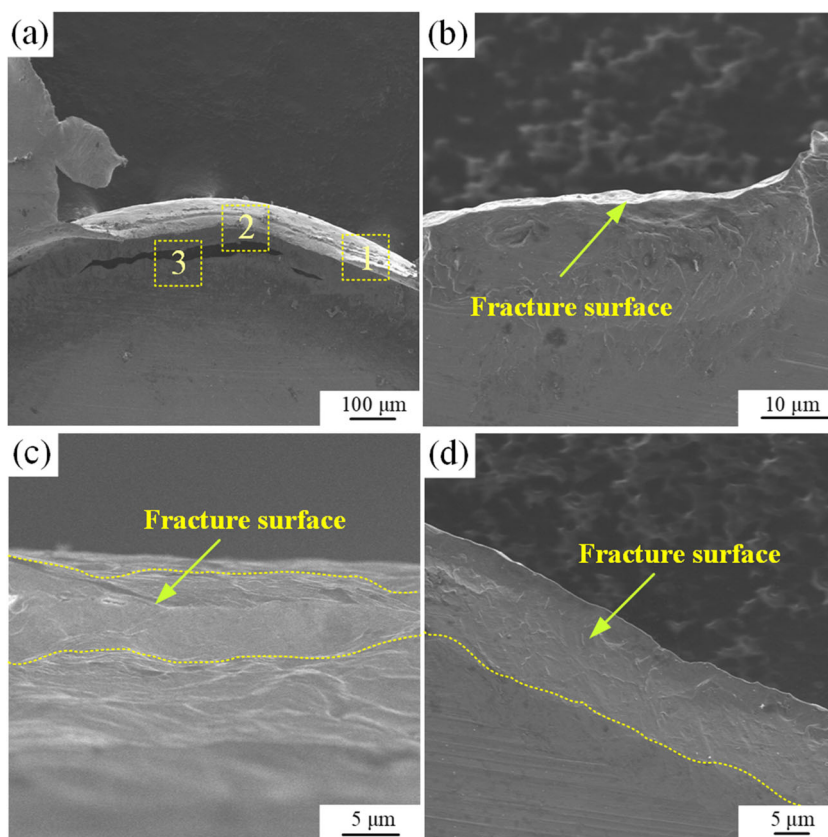
#### 4.3.4 Mixed fracture

Figure 11 presents the fracture morphology on both the bottom corner and neck of one joint, named mixed fracture. The corresponding clinching conditions are as follows:  $I = 4.67 \times 10^{12} \text{ W/m}^2$ ;  $d_G = 27 \text{ }\mu\text{m}$ ;  $t_U = 30 \text{ }\mu\text{m}$ ;  $d_S = 2.0 \text{ mm}$ ;  $H = 100 \text{ }\mu\text{m}$ ; and number of laser pulses, 45. Before SEM examination, joining partner II has also been carefully removed to better observe the fracture site. As seen in Fig. 11a, regions 1 and 2 represent fracture on the neck, while region 3 is located at the bottom corner. From Fig. 11b–d, it is evident that there is severe thinning on the fracture surface, suggesting that significant plastic deformation occurs prior to fracture. Due to the confinement of the blank holder, the formation of the joint is realized by bulging forming of pure copper foil under the effect of tensile stresses, and thus, the metal foil becomes thinner with the increase of laser pulses until fracture appears. In the present experiments, it is noted that the mixed fracture mode accounts for the majority of fractured specimens.

**Fig. 10** Force acting on the region in contact with the upper corner of joining partner II



**Fig. 11** Morphology of mixed fracture. **a** General view of the fracture region. **b** Amplification of region 1 in **a**. **c** Amplification of region 2 in **a**. **d** Amplification of region 3 in **a**



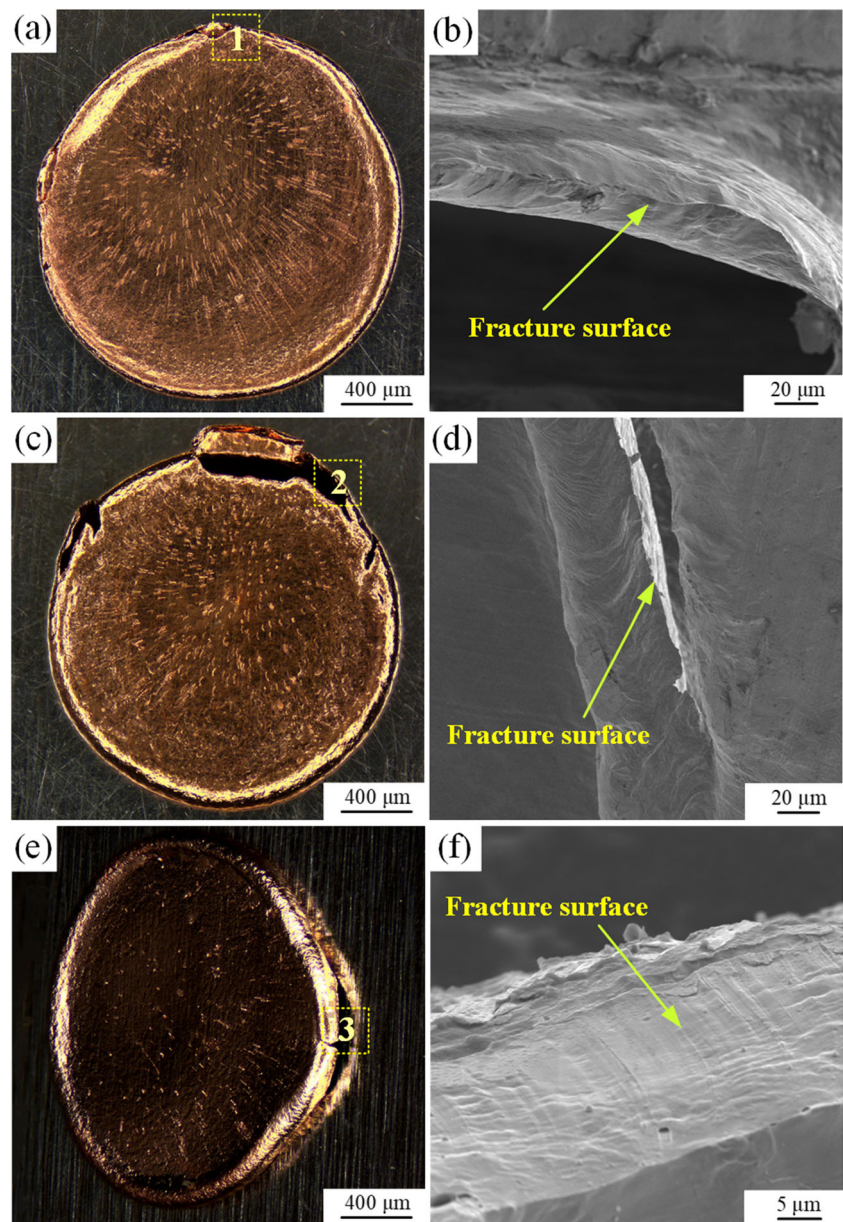
#### 4.4 Effect of laser power density on fracture modes

The laser power density determines the interaction of the pulsed laser beam and the absorbent coating and thus directly involves the amplitude of the induced shock wave pressure. Therefore, it is one of essential process parameters for joint formation in the laser shock hole-clinching process and is necessary to understand its influence on fracture modes. In the experiments, three laser power densities of  $5.10 \times 10^{12}$ ,  $5.52 \times 10^{12}$ , and  $6.37 \times 10^{12}$  W/m<sup>2</sup> corresponding to the pulsed laser energy of 120, 130, and 150 mJ were applied. The other clinching conditions are as follows:  $d_G = 13 \mu\text{m}$ ,  $t_U = 30 \mu\text{m}$ ,  $d_S = 2.0 \text{ mm}$ , and  $H = 100 \mu\text{m}$ . Figure 12 shows the typical morphology of the fracture surface under various laser power densities. As seen in Fig. 12a, the crack appears on the bottom corner at  $5.10 \times 10^{12}$  W/m<sup>2</sup>, and its SEM observation confirms that the fracture site becomes thinner under the action of tensile stress; refer to Fig. 12b. While the laser power density is increased to  $5.52 \times 10^{12}$  W/m<sup>2</sup>, it is noted that the fracture of the joint is more serious and occurs on both the bottom corner and neck region, as shown in Fig. 12c. The amplified examination also exhibits the thinning phenomenon in this case from Fig. 12d. Furthermore, when a laser power density of  $6.37 \times 10^{12}$  W/m<sup>2</sup> has been applied, it is found that fracture occurs with few laser

pulses. Although the crack also appears on the neck shown in Fig. 12e, the SEM result presents a different morphology compared with those in Fig. 12b and d. From Fig. 12f, it is clearly seen that the fracture surface seems smooth and is obviously formed by shear stress, indicating that the development of crack is on the base of shear fracture mechanism. According to the fracture surface analysis, it is concluded that the fracture mode varies from a tensile fracture mode on the bottom corner to a mixed tensile fracture mode and then to a shear fracture mode on the neck with the enhancement of the laser power density, as summarized in Table 2.

The amplitude of the shock wave pressure under the given laser power densities can be estimated according to Eq. (4). In the present research, the shock impedance of quartz glass and pure copper is  $1.31 \times 10^7$  kg/m<sup>2</sup> s and  $4.18 \times 10^7$  kg/m<sup>2</sup> s, respectively [33]. Thus, the calculated shock wave pressure is increased from 1.78 to 2.01 GPa while the laser power density is enhanced from  $5.10 \times 10^{12}$  to  $6.37 \times 10^{12}$  W/m<sup>2</sup>. Considering the stress state in Fig. 10, the strengthened shock wave pressure provides a high stress gradient within the material near the upper corner of joining partner II [20, 22]. In this case, the corresponding material tends to fracture in shear fracture mode under the effect of high-amplitude shock wave pressure.

**Fig. 12** Morphology of fracture surface under various laser power densities with pure copper foil of 30 μm in thickness. **a**  $I = 5.10 \times 10^{12}$  W/m<sup>2</sup>. **b** Amplification of region 1 in **a**. **c**  $I = 5.52 \times 10^{12}$  W/m<sup>2</sup>. **d** Amplification of region 2 in **c**. **e**  $I = 6.37 \times 10^{12}$  W/m<sup>2</sup>. **f** Amplification of region 3 in **e**



**4.5 Effect of initial grain size of joining partner I on fracture modes**

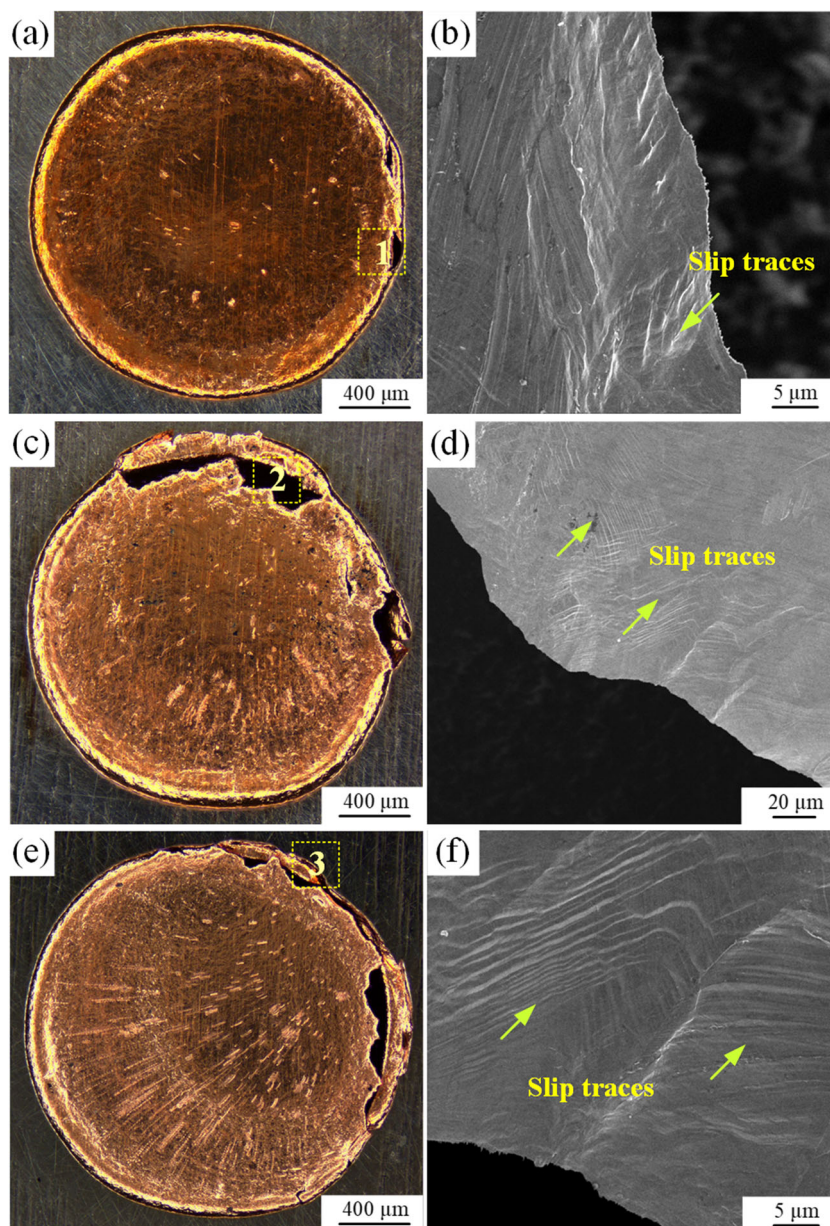
Pure copper foils with three initial grain sizes of 13, 17, and 27 μm were prepared in advance aiming to identify the grain size effect on the fracture mode of joints. The other clinching

conditions are as follows:  $I = 5.52 \times 10^{12}$  W/m<sup>2</sup>,  $t_U = 30$  μm,  $d_S = 2.0$  mm, and  $H = 100$  μm. Figure 13 shows the typical morphology of the fracture surface with various initial grain sizes. In the case of 13 μm, the fracture site is located at the bottom corner, whereas the cracks appear on both the bottom corner and neck of the joint with 17 μm, as shown in Fig. 13a

**Table 2** Variation of fracture modes related to laser power density

Laser power density ( $\times 10^{12}$ W/m <sup>2</sup> )	Fracture mode	Fracture mechanism
5.10	Bottom corner fracture	Tensile
5.52	Mixed fracture	Tensile
6.37	Neck fracture	Shear

**Fig. 13** Morphology of fracture surface with various initial grain sizes of joining partner I. **a**  $d_G = 13 \mu\text{m}$ . **b** Amplification of region 1 in **a**. **c**  $d_G = 17 \mu\text{m}$ . **d** Amplification of region 2 in **c**. **e**  $d_G = 27 \mu\text{m}$ . **f** Amplification of region 3 in **e**



and **c**. The SEM examination confirms that the metal foil loses its integrity due to the excessive thinning, and significant plastic deformation occurs prior to fracture with the evidences of slip traces; refer to Fig. 13**b** and **d**. Moreover, while the grain size enlarges from 17 to 27  $\mu\text{m}$ , it is noted that the fracture site also lies in the bottom corner and neck of the joint but the size of fracture region becomes large, as seen in Fig. 13**e**. According to the empirical Hall-Petch relationship, the flow stress of materials decreases with the increase in grain size, implying that larger plastic deformation can be achieved with coarse grains, and, thus the final fracture seems more serious [34]. The further observation shows that the metal foil of 27  $\mu\text{m}$  in initial grain size is separated also due to excessive thinning from Fig. 13**f**. Table 3 summarizes the variation of

fracture modes related to the initial grain size of joining partner I.

#### 4.6 Effect of thickness of joining partner I on fracture modes

Due to the fact that fracture always occurs on joining partner I, the effect of the thickness of joining partner I on fracture modes is of concern. Figure 14 presents the typical morphology of a fracture surface under various laser power densities with pure copper foil of 50  $\mu\text{m}$  in thickness. Before laser shock experiments, the 50  $\mu\text{m}$  pure copper foil was also annealed in a vacuum furnace at a temperature of 450  $^{\circ}\text{C}$  for 1 h, and the average grain size in the thickness direction was

**Table 3** Variation of fracture modes related to the initial grain size of joining partner I

Initial grain size of pure copper ( $\mu\text{m}$ )	Fracture mode	Fracture mechanism
13	Bottom corner fracture	Tensile
17	Mixed fracture	Tensile
27	Mixed fracture	Tensile

about  $14 \mu\text{m}$ . The applied laser spot diameter was  $2.0 \text{ mm}$ , and the spacer height was  $100 \mu\text{m}$ . From Fig. 14a–c, it can be seen that the fracture mode varies from a tensile fracture mode on the bottom corner to a mixed tensile fracture mode while the laser power density is enhanced from  $5.10 \times 10^{12}$  to  $6.37 \times 10^{12} \text{ W/m}^2$ . It is found that the shear fracture on the neck of the joint finally appears at  $I = 8.49 \times 10^{12} \text{ W/m}^2$  ( $E = 200 \text{ mJ}$ ), as shown in Fig. 14d. Thus, the pure copper foil of  $50 \mu\text{m}$  in thickness exhibits the same variation trend compared with the corresponding change for pure copper foil with a thickness of  $30 \mu\text{m}$ . This phenomenon further confirms that laser power density has an important impact on the deformation and fracture behavior of joining partner I in the laser shock hole-clinching process.

#### 4.7 Effect of laser spot diameter on fracture modes

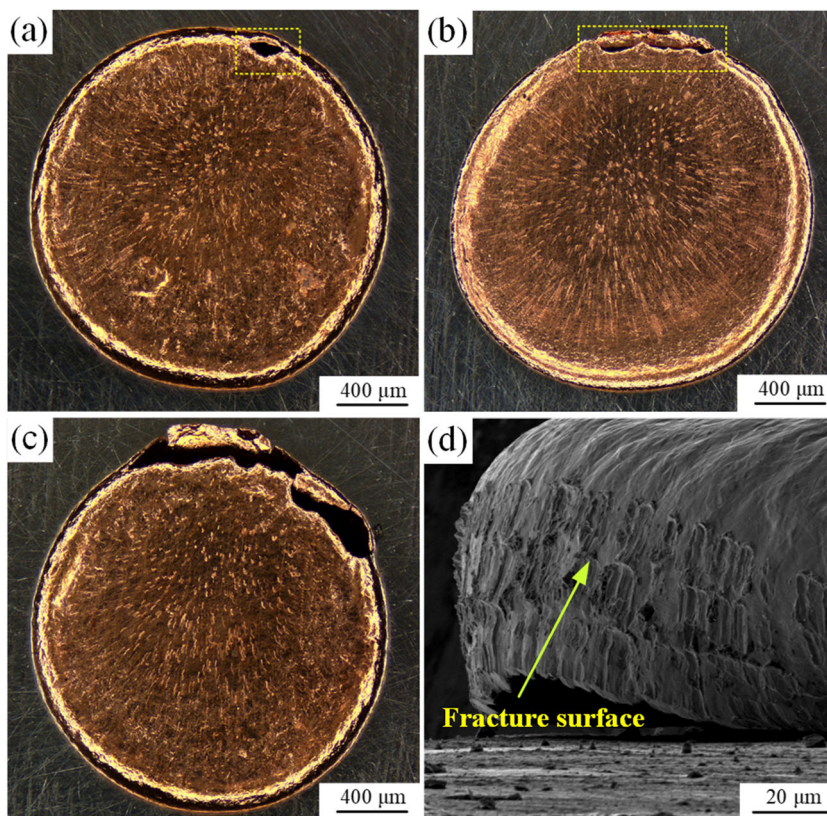
Figure 15 presents the typical morphology of the fracture surface at various laser spot diameters. The other clinching

conditions are as follows:  $I = 5.52 \times 10^{12} \text{ W/m}^2$ ,  $d_G = 13 \mu\text{m}$ ,  $t_U = 30 \mu\text{m}$ , and  $H = 100 \mu\text{m}$ . The morphology of fracture surface at  $d_S = 2.0 \text{ mm}$  ( $M = 1$ ) refers to Fig. 12c and d. It is noted that although the matching relationship between the laser spot diameter and pre-pierced hole diameter changes, the fracture site always lies in both the bottom corner and the neck of the clinched joint. Therefore, the occurrence of mixed fracture under three cases of  $M$  values suggests that the material of joining partner I undergoes severe material flowing, leading to the serious reduction in the thickness in these regions. The determination of the  $M$  value needs to be concerned with both the joint forming quality and the operation convenience.

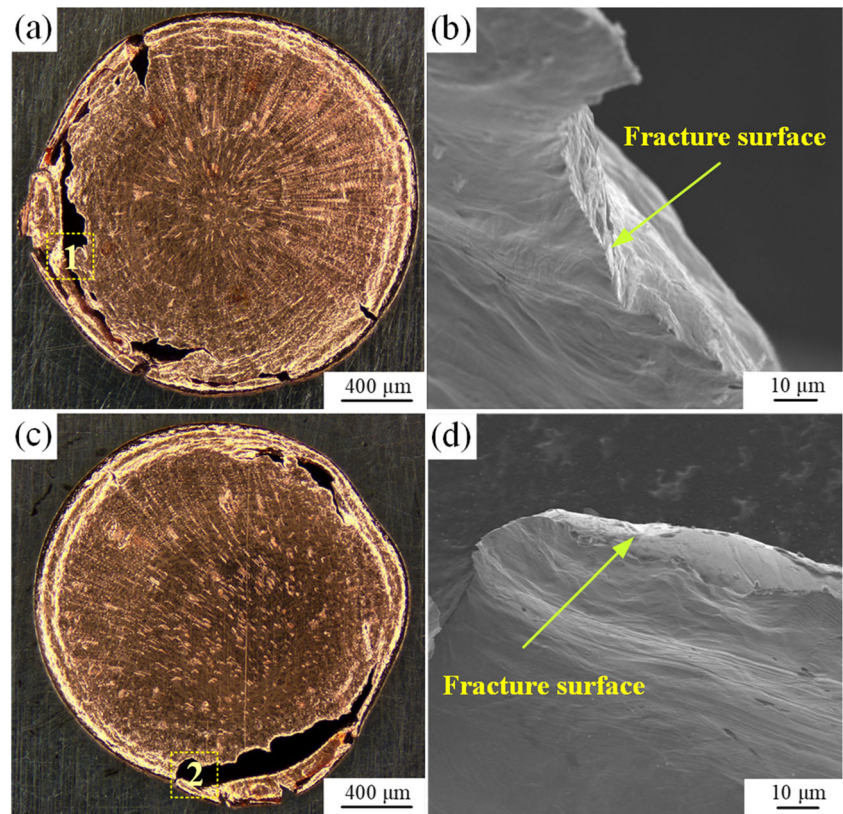
#### 4.8 Effect of spacer height on fracture modes

Figure 16 shows the typical morphology of the fracture surface with various spacer heights. The other clinching conditions are as follows:  $I = 5.52 \times 10^{12} \text{ W/m}^2$ ,  $d_G = 13 \mu\text{m}$ ,  $t_U =$

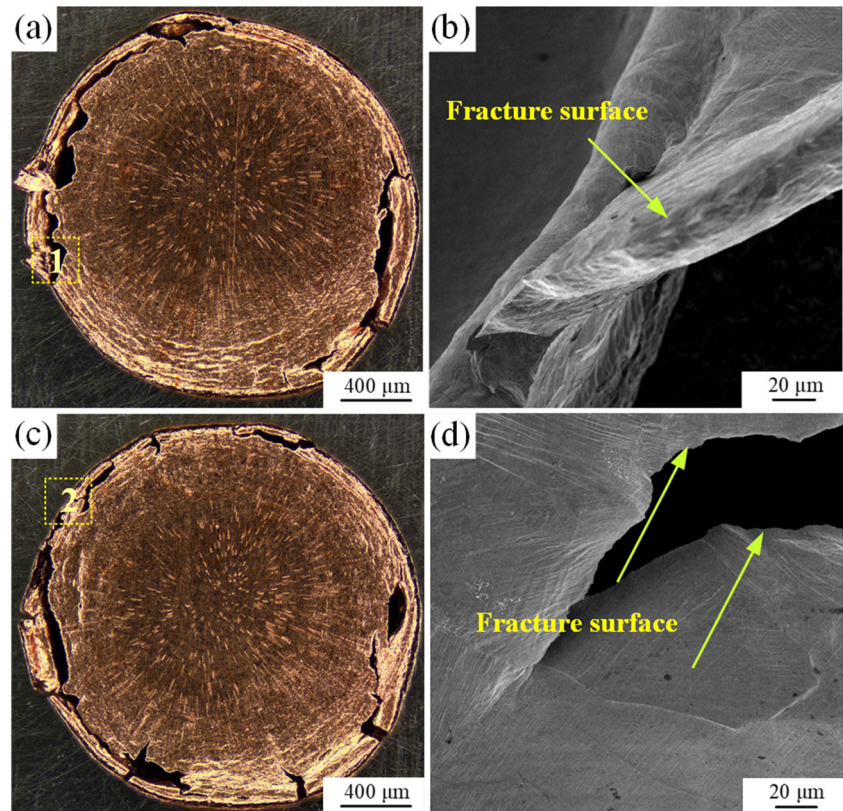
**Fig. 14** Morphology of fracture surface under various laser power densities with pure copper foil of  $50 \mu\text{m}$  in thickness. **a**  $I = 5.10 \times 10^{12} \text{ W/m}^2$ . **b**  $I = 5.52 \times 10^{12} \text{ W/m}^2$ . **c**  $I = 6.37 \times 10^{12} \text{ W/m}^2$ . **d** Amplification of fracture surface at  $I = 8.49 \times 10^{12} \text{ W/m}^2$



**Fig. 15** Morphology of fracture surface at various laser spot diameters. **a**  $d_S = 1.8$  mm ( $M < 1$ ). **b** Amplification of region 1 in **a**. **c**  $d_S = 2.2$  mm ( $M > 1$ ). **d** Amplification of region 2 in **c**



**Fig. 16** Morphology of fracture surface with various spacer heights. **(a)**  $H = 150$  μm. **b** Amplification of region 1 in **a**. **c**  $H = 200$  μm. **d** Amplification of region 2 in **c**



30  $\mu\text{m}$ , and  $d_s = 2.0$  mm. The morphology of the fracture surface at  $H = 100$   $\mu\text{m}$  refers to Fig. 12c and d. Based upon the experimental observation, the mixed fracture mode always appears as the spacer height enlarges from 100 to 200  $\mu\text{m}$ . As shown in Fig. 1a, an increasing spacer height indicates that the height of the interlock structure becomes larger, implying that more materials are needed to form a form-fit joint. Due to the confinement of the blank holder, it is difficult for the pure copper foil outside the pre-pierced hole to flow into the cavity, resulting in a major reduction in thickness and final fracture on both the bottom corner and neck of the joint.

## 5 Conclusions

In this paper, the fracture mode of Cu-Fe joints by laser shock hole-clinching was experimentally investigated. The characteristics of the fracture surface morphology of joints under critical process parameters were examined based on OM and SEM observations. The following conclusions are drawn from this research:

1. The temperature increase caused by high-strain rate plastic deformation during the laser shock hole-clinching process can be ignored, and thus, it has no impact on the fracture behavior of the joining partners.
2. Fracture always occurs on joining partner I, and it can be divided into four modes, that is, bottom surface fracture, bottom corner fracture, neck fracture, and mixed fracture. Among these modes, fracture on the bottom surface is seldom seen but mixed fracture accounts for most of cracked specimens. Neck tensile fracture rarely appears alone, and it usually exists accompanied by fracture on the bottom corner.
3. For the concerned laser power densities, the fracture mode varies from a tensile fracture mode on the bottom corner to a mixed fracture mode and then to a shear fracture mode on the neck with the enhancement of laser power density. The laser-induced shock wave pressure is responsible for the variation of fracture modes under different laser power densities.
4. The initial grain size of joining partner I has a significant impact on the fracture mode of clinched joints. The fracture mode varies from bottom corner fracture to mixed fracture in relation to the change of mechanical properties of metal foil with an enlarged grain size.
5. The same varying trend of fracture modes is observed for the pure copper foil of 30 and 50  $\mu\text{m}$  in thickness. In addition, the mixed fracture mode always appears with the enlargement of both laser spot diameter and spacer height.

Additionally, the present research focuses on the classification of fracture modes of Cu-Fe joints in laser shock hole-

clinching. Although the effect of critical process parameters on fracture modes has been studied, a design of experiment is needed to thoroughly understand the variation of fracture modes with the changing of laser shock hole-clinching conditions. Moreover, it is noticeable that the thickness of absorbent coating plays an essential role in laser material processes, and thus, the effect of the thickness of absorbent coating on fracture modes should be given a systematic investigation. In addition, it is necessary to carry out finite element analysis to capture the evolution characteristic of cracks aiming to deeply understand the fracture behavior of metal foils in the laser shock hole-clinching process.

**Authors' contribution** Chao Zheng: Conceptualization, writing—original draft preparation, writing—revision  
Shushuai Liu: Methodology, writing—revision  
Yunhu Zhu: Investigation  
Yiliang Zhang: Investigation, writing—original draft preparation  
Guoqun Zhao: Supervision, writing—review  
Zhong Ji: Writing—review

**Funding** This work is supported by the National Natural Science Foundation of China (No. 52075299), Natural Science Foundation of Shandong Province (No. ZR2020ME149), and the Fundamental Research Funds of Shandong University (2018JC042).

**Availability of data and material** Not applicable.

**Code availability** Not applicable.

## Declarations

**Conflict of interest** The authors declare no competing interests.

## References

1. Tanaka S, Bataev I, Nishi M, Balagansky I, Hokamoto K (2019) Micropunching large-area metal sheets using underwater shock wave: experimental study and numerical simulation. *Int J Mach Tools Manuf* 147:103457. <https://doi.org/10.1016/j.ijmactools.2019.103457>
2. Choi DC, Kim HS (2020) Performance evaluation of laser shock micro-patterning process on aluminum surface with various process parameters and loading schemes. *Opt Lasers Eng* 124:105799. <https://doi.org/10.1016/j.optlaseng.2019.105799>
3. Ji Z, Liu R, Wang DG, Zhang MH, Su QC (2008) A micro clinching method and its device for joining ultrathin sheets with pulsed laser. Chinese Patent ZL200810014018.1.
4. Veenaas S, Vollertsen F (2015) Forming behavior during joining by laser induced shock waves. *Key Eng Mater* 651–653:1451–1456. <https://doi.org/10.4028/www.scientific.net/KEM.651-653.1451>
5. Wang X, Li C, Ma YJ, Shen ZB, Sun XQ, Sha CF, Gao S, Li LY, Liu HX (2016) An experimental study on micro clinching of metal foils with cutting by laser shock forming. *Materials* 9:571. <https://doi.org/10.3390/ma9070571>

6. Wang X, Li XD, Li C, Shen ZB, Ma YJ, Liu HX (2018) Laser shock micro clinching of Al/Cu. *J Mater Process Technol* 258:200–210. <https://doi.org/10.1016/j.jmatprotec.2018.04.005>
7. Wang XY, Ji Z, Wang JF, You SX, Zheng C, Liu R (2018) An experimental and numerical study on laser shock clinching for joining copper foil and perforated stainless steel sheet. *J Mater Process Technol* 258:155–164. <https://doi.org/10.1016/j.jmatprotec.2018.03.025>
8. Veenas S, Vollertsen F (2014) High speed joining process by laser shock forming for the micro range. 6th International Conference on High Speed Forming, Daejeon, Korea: 97–105. <https://doi.org/10.17877/DE290R-854>
9. Veenas S, Wielage H, Vollertsen F (2014) Joining by laser shock forming: realization and acting pressures. *Prod Eng Res Devel* 8: 283–290. <https://doi.org/10.1007/s11740-013-0521-z>
10. Wang XY, Ji Z, Liu R, Zheng C (2018) Making interlock by laser shock forming. *Opt Laser Technol* 107:331–336. <https://doi.org/10.1016/j.optlastec.2018.06.011>
11. You SX, Wang XY, Ji Z, Zheng C, Zhang GF, Liu R (2019) Making line undercut structure by incremental laser shock forming. *Int J Precis Eng Manuf* 20:1289–1296. <https://doi.org/10.1007/s12541-019-00141-w>
12. Li XD, Wang X, Shen ZB, Ma YJ, Liu HX (2019) An experimental study on micro-shear clinching of metal foils by laser shock. *Materials* 12:1422. <https://doi.org/10.3390/ma12091422>
13. Li J, Gao H, Cheng GJ (2010) Forming limit and fracture mode of microscale laser dynamic forming. *J Manuf Sci Eng* 132:061005. <https://doi.org/10.1115/1.4002546>
14. Wielage H, Vollertsen F (2011) Analysis of fracture behavior in plastic shaping by laser shock forming, 10th International Conference on Technology of Plasticity. Aachen, Germany, pp 1–4
15. Liu Z, Zheng C, Song LB, Ji Z (2019) Forming limit and fracture mode in multiple-pulse laser shock micro-bulging process. *Chinese J Lasers* 46:0302004. <https://doi.org/10.3788/CJL201946.0302004>
16. Wang X, Sun K, Ma YJ, Shen ZB, Liu F, Liu HX (2019) Experimental investigation on laser shock micro hydraulic bulging of copper foil. *Opt Laser Technol* 115:390–397. <https://doi.org/10.1016/j.optlastec.2019.02.048>
17. Zhang QL, Wang R, Hong YX, Wu TD, Qian Y, Zhang YK (2014) Study on laser shock forming and fracture behavior of metal sheet. *Chinese J Lasers* 41:0403010. <https://doi.org/10.3788/CJL201441.0403010>
18. Jiang YF, Sha DL, Jiang WF, He YZ, Jin H (2019) A study on failure mechanisms and formability of aluminum alloy sheets under laser shock forming. *Int J Adv Manuf Technol* 101:451–460. <https://doi.org/10.1007/s00170-018-2765-4>
19. Zheng C, Ji Z, Song LB, Fu J, Zhu YH, Zhang JH (2015) Variation of fracture mode in micro-scale laser shock punching. *Opt Laser Technol* 72:25–32. <https://doi.org/10.1016/j.optlastec.2015.03.009>
20. Shen ZB, Liu HX, Wang X, Wang CT (2016) Improving the forming capability of laser dynamic forming by using rubber as a forming medium. *Appl Surf Sci* 369:288–298. <https://doi.org/10.1016/j.apsusc.2016.02.063>
21. Shen ZB, Zhang JD, Li P, Liu HX, Yan Z, Ma YJ, Wang X (2019) Deformation and fracture behaviors of copper sheet in laser dynamic flexible forming. *J Manuf Process* 37:82–90. <https://doi.org/10.1016/j.jmapro.2018.11.015>
22. Li M, Zhang XQ, Li SZ, Wang HT, Chen B, Tong JY, Fang GW, Wei W (2019) Effect of the pressure on fracture behaviors of metal sheet punched by laser-induced shock wave. *Int J Adv Manuf Technol* 102:497–505. <https://doi.org/10.1007/s00170-018-3197-x>
23. Boakye-Yiadom S, Bassim N (2018) Microstructural evolution of adiabatic shear bands in pure copper during impact at high strain rates. *Mater Sci Eng A* 711:182–194. <https://doi.org/10.1016/j.msea.2017.11.027>
24. Tiamiyu AA, Odeshi AG, Szpunar JA (2018) Multiple strengthening sources and adiabatic shear banding during high strain-rate deformation of AISI 321 austenitic stainless steel: effects of grain size and strain rate. *Mater Sci Eng A* 711:233–249. <https://doi.org/10.1016/j.msea.2017.11.045>
25. Bobbili R, Madhu V, Gogia AK (2016) Tensile behaviour of aluminium 7017 alloy at various temperatures and strain rates. *J Mater Res Technol* 5:190–197. <https://doi.org/10.1016/j.jmrt.2015.12.002>
26. Johnson GR, Cook WH (1983) A constitutive model and data for metals subjected to large strains, high strain rates and high temperatures, 7th International Symposium on Ballistics. Hague, Netherlands, pp 541–547
27. Fabbro R, Fournier J, Ballard P, Devaux D, Virmont J (1990) Physical study of laser-produced plasma in confined geometry. *J Appl Phys* 68:775–784. <https://doi.org/10.1063/1.346783>
28. Ryazanov AI, Pavlov SA, Kiritani M (2003) Effective temperature rise during propagation of shock wave and high-speed deformation in metals. *Mater Sci Eng A* 350:245–250. [https://doi.org/10.1016/S0921-5093\(02\)00711-6](https://doi.org/10.1016/S0921-5093(02)00711-6)
29. Wielage H, Vollertsen F (2011) Classification of laser shock forming within the field of high speed forming processes. *J Mater Process Technol* 211:953–957. <https://doi.org/10.1016/j.jmatprotec.2010.07.012>
30. Ye YX, Xuan T, Lian ZC, Feng YY, Hua XJ (2015) Investigation of the crater-like microdefects induced by laser shock processing with aluminum foil as absorbent layer. *Appl Surf Sci* 339:75–84. <https://doi.org/10.1016/j.apsusc.2015.02.111>
31. Lambiase F, Di Ilio A (2016) Damage analysis in mechanical clinching: experimental and numerical study. *J Mater Process Technol* 230:109–120. <https://doi.org/10.1016/j.jmatprotec.2015.11.013>
32. Lambiase F, Di Ilio A, Paoletti A (2015) Joining aluminium alloys with reduced ductility by mechanical clinching. *Int J Adv Manuf Technol* 77:1295–1304. <https://doi.org/10.1007/s00170-014-6556-2>
33. Zheng C, Sun S, Ji Z, Wang W, Liu J (2010) Numerical simulation and experimentation of micro scale laser bulge forming. *Int J Mach Tools Manuf* 50:1048–1056. <https://doi.org/10.1016/j.ijmactools.2010.08.012>
34. Zheng C, Zhang X, Liu Z, Ji Z, Yu X, Song LB (2018) Investigation on initial grain size and laser power density effects in laser shock bulging of copper foil. *Int J Adv Manuf Technol* 96: 1483–1496. <https://doi.org/10.1007/s00170-018-1722-6>

**Publisher's note** Springer Nature remains neutral with regard to jurisdictional claims in published maps and institutional affiliations.